ORIGINAL ARTICLE

Finite Element Analysis of Femoral Strains in Older Adults During Stair Ascent and Descent

Chen Deng[1] · Jason C. Gillette[2] · Timothy R. Derrick[2]

Abstract

Purpose Understanding the femur load environment during daily activity is necessary for the understanding of risk of femoral pain, pain related falls, and femoral fractures, which could help the design of osteogenic exercises or the preventative methods for older adults.

Methods Using the finite element femur analysis, this study was to estimate the femoral strains at 9 cross-sections along the long axis of femur for stair ascent and descent ($n = 17$; age: 50–65 years). Motion analysis and inverse dynamics were combined with musculoskeletal modelling and optimization, then were used as input to a 3-D femur model to estimate femoral strains. Strains at the hip contact force peaks were calculated.

Results The compressive and tensile strains during stair descent were greater than ascent for all or most cross-sections, especially for the proximal cross-sections of the femur: stair ascent produced -324.0 ± 103.8 to -483.7 ± 191.0 µε compressive strains and descent produced -608.8 ± 288.4 to 1016.0 ± 444.1 µε; stair ascent produced 336.2 ± 105.4 to 391.8 ± 136.9 µε tensile strains and descent produced 546.9 ± 252.8 to 741.7 ± 333.6 µε.

Conclusion Strains represent the material deformation effect on the bone due to the sum of all the bone external loads. Using bone strains could help future studies analyze load conditions in a more comprehensive way for other physical activities, which predicts the risk of stress fractures and tests if alternative methods (gait type change) could reduce stress and strain effectively.

Keywords Femoral cross-sections · Finite element method · Bone strains · Stair ascent and descent · Older adults

Introduction

The femoral fractures could occur at any regions (proximal, shaft, or distal femur) and lead to serious health issues [8, 23, 24]. The proximal femoral fracture at the femoral head/neck, intertrochanteric, and subtrochanteric regions [8] could result in reduced life expectancy and dramatic deterioration in health and social conditions for older adults [38]. Distal femur fractures are the second most frequent femoral fractures [29, 33], and the mortality rate for this type of fractures is comparable to that of hip fractures [12, 40]. Femoral shaft fractures could be less common but still a concern on bisphosphonates for osteoporosis and result in serious health issues for older populations [2, 26, 30]. All femoral fractures occur with greater frequency in older populations could be caused by osteoporotic issues combining with low-energy mechanisms [17] or stress/fatigue fractures [8, 37]. For older individuals, more femoral load may lead to hip joint and femoral pain issues. Recently, more hip joint/femoral pain and pain related falls are reported during stair navigation; about 30% of older individuals suffered at least one fall in life time, and 20%–30% of falls led to the serious injuries including femoral fractures [19, 35].

Finite element method (FEM), musculoskeletal modeling, and force estimation could be used in the analysis of the bone load environment and estimation of the fracture risks. This material analysis provides the estimation of stress/strain for the whole femur, which represents the effect of all the external loads of the femur (e.g. joint

✉ Chen Deng
dengchen@bsu.edu.cn

1 Division of Sport Biomechanics, School of Sport Science, Beijing Sport University, No. 48, Xinxi Road, Beijing 100084, People's Republic of China

2 Department of Kinesiology, Iowa State University, Ames, IA, USA

contact forces and muscular forces). Most femur models used in FEM were derived from CT/MRI scans of bone specimens [22, 44], and the models with individual's bone material property and geometry could predict the loading condition in a more realistic way. Early applications for these models were loading tests using artificial load acting on the fixed points of the model to simulate standing, walking or landing tasks. The load conditions and failure criteria, bone failure theory testings were fulfilled by finite element models [9, 22]. It is well known that femur model with simplified muscle models resulted in significantly inaccurate analysis [11, 39], so the femur model with all attaching muscle forces are necessary to reflect the accuracy of the stress/strain estimation [1, 36].

Previous research investigated load environments for several specific regions of the femur, especially for the femoral neck [3, 5, 10, 21], but few studies focused on the load environment for other regions of the femur [27]. Due to the seriousness of femoral fractures at the shaft and distal regions, investigating the strain conditions throughout the whole femur could be helpful to understand the etiology and risk for femoral pain, pain related falls and fractures; the effects from the external loads could be detected during different physical activities. For stair ascent and descent, the analysis throughout the whole femur could be helpful to figure out which activity could generate more mechanical loads on the femur and become risk factors for stress fracture, femoral pain and pain related falls [20, 35]. According to the load environment for the femur, future research could design more strategies to reduce femoral load during stair ascent and descent to reduce the femoral pain and pain related falls.

The purpose of this study was to examine the femoral strains during stair ascent and descent, which could give more information about the load environments for femur for older populations. In this study, a femur model was used for finite element analysis to analyze the strains for the whole femur. Along the long axis of the model, 9 cross-sections at each 10% of the total length (Fig. 1) were analyzed to compare strains at each cross-section between stair ascent and descent. It is assumed that stair descent would produce more femoral strains than ascent since more cases of femoral pain and pain related falls were reported during stair descent.

In this analysis, both the minimal principal strains (compressive) and the maximal principal strains (tensile) on the femur were estimated. These strain estimations during stair ascent and descent can reveal the load environment of the whole femur and analyze the femoral loads that could be responsible for femoral pain, its related falls and injuries.

Methods

For the repeated-measures ANOVA with a power of 0.80, 16–17 participants were needed according to G*Power (input requirement: default effect size as 0.30, α as 0.05). Seven male (age: 60 ± 6 years; mass: 75 ± 14 kg; height: 1.73 ± 0.05 m) and 10 female subjects (age: 57 ± 5 years; mass: 67 ± 8 kg; height: 1.67 ± 0.05 m), who were free from
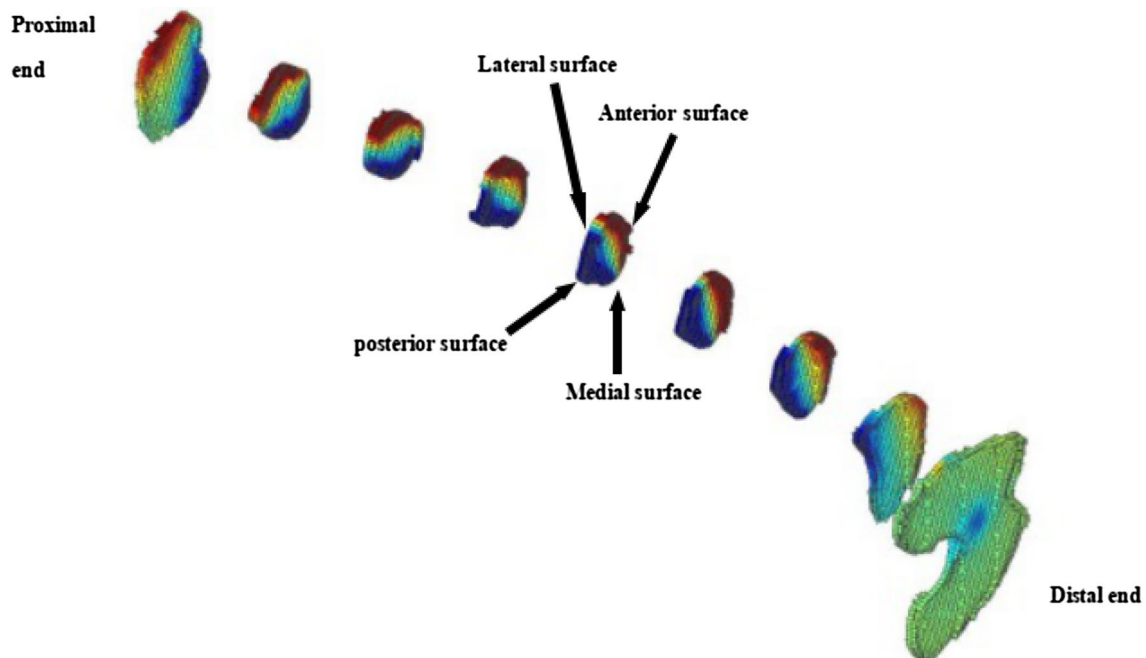

Fig. 1 The finite element analysis for the cross section area of whole femur at the spot of each 10% along the femur length (from 10% to 90%)

lower limb injuries, participated in this study. Before participation, each participant signed a written informed consent which had been approved by the Iowa State University Human Subjects Review Board.

Body mass, height, and the anthropometric of right lower extremity segments (lengths, widths, and circumferences) were measured. Eighteen reflective markers with double sides adhesive tape were placed on anatomical landmarks of the trunk, pelvis, and right lower extremity with a minimum of 3 markers per segment: toe (second metatarsophalangeal joint), heel and lateral foot (lateral side of the mid-foot) markers for the foot segment; anterior (mid of the anterior leg), posterior leg (posterior lower leg) and medial/lateral ankle markers (the medial and lateral malleolus) for the leg segment; anterior thigh (mid of the anterior thigh), lateral thigh (mid of the lateral thigh), right hip (right greater trochanter) and medial/lateral knee markers (medial and lateral condyle) for the thigh segment; left hip (left greater trochanter), right/left ASIS (anterior superior iliac spine), right/left PSIS (posterior superior iliac spine), and sacrum for the pelvis segment; medial/lateral ankle can be considered both in the foot and leg segments, medial/lateral knee can be considered both in the leg and thigh segments. All anthropometric measurements and marker placements were performed by the same researcher before the testing; the segment masses, center of mass locations, and moments of inertia for each segment were obtained based on anthropometric measurements, the kinematics of the hip/knee/ankle joint centers were obtained from the calculation based on the marker kinematics [43].

A static trial was collected with the subject in anatomical position to estimate joint center locations by the markers, and then the medial ankle and knee markers were removed. All subjects performed five trials of stair ascent and five trials of descent (three-step staircase, height of each stair: 19 cm) at their normal comfortable speed without any external support (e.g. handrails or canes). For each trail, participants took the 1st step with left leg, and the 2nd step was taken with the right leg. During the 2nd step, the right foot contacted the force platform on the 2nd level of the staircase. AMTI force platforms (1600 Hz, AMTI, Watertown, MA, USA) were placed on the two lower stairs to measure ground reaction forces. Motion data (kinematics of markers) were collected using an 8-camera system (160 Hz, Vicon MX, Centennial, CO, USA).

Ground reaction forces and motion data were filtered using a low-pass Butterworth filter with a cutoff frequency of 6 Hz [45]. The stance phase cycle for stair ascent/descent began with right foot first contacting the force platform and finished with its toe-off. All gait cycles were normalized into a percentage of the stance phase. A rigid body model was used with inverse dynamics procedures to estimate three-dimensional joint moments and reaction forces at the ankle, knee, and hip in the global coordinate system, and then transformed into the coordinate system of the proximal segment at each joint.

A musculoskeletal model based on the joint and muscle definitions of Arnold [4] was implemented in Matlab to estimate the dynamic muscle–tendon length, velocity adjusted maximal muscle forces, muscle moment arms and orientations for 44 lower limb muscles (scaled by individual's anthropometric measurements). The three dimensional segment angles obtained during the trials were used in the model to estimate the above parameters. Using static optimization method, a set of muscle forces solution was selected based on these requirements: (1) minimizing the sum of the squared muscle stresses [16]; (2) balancing with the joint external moments, including the sagittal plane hip, knee and ankle moments, frontal plane hip moment and the transverse plane hip and ankle moments. This best solution was also constrained by the maximal dynamic muscle forces estimated with the musculoskeletal model:

$$\text{Min} \sum_{i=1}^{44} (F_i/A_i)^2 \text{ Subject to}: r_{ij} \times F_i = M_j 0 \leq F_i \leq \text{Max dynamic } F_i$$

For the ith muscle: F_i is estimated muscle force, A_i is the cross-sectional area, r_{ij} is the moment arm for the jth joint moment, and M_j is the jth joint moment.

The 3-demensional hip joint reaction forces were summed with muscle forces from muscles that crossed the hip joint to obtain hip joint contact forces. The 3-demensional hip joint contact forces were then acting on the femoral head of the femur model.

The finite element model for the whole femur was provided by VAKHUM database [42]. The model was developed by the clinical CT scans for the femur from a female cadaver (age: 99-years; mass: 55 kg; height: 1.55 m), and the apparent density was calculated according to Schileo et al. [36]. For the model, the acquisition setting of the CT scan was 120 kVp and 200 mAs, and images were reconstructed with a slice thickness of 2.7 mm and an in-plane pixel resolution of 0.840 mm. The finite element model from the database contained 104,945 linear hexahedral elements with 115,835 degrees of freedom (or nodes) with a default element edge length as 2.0 mm. Principal stresses, and principal strains had less than 3% change when increasing element edge length from 2.0 to 3.0 mm, which guaranteed the adequate convergence at the refinement.

The finite element model was scaled by the individual thigh length in longitudinal direction, and then scaled by the length·diameter$^2 \propto$ body mass [28] in radial direction. The material property was justified by the gender specific correlations between Young's modulus and age which developed from Burstein et al. [7]. For the whole femur, the isotropic material property, including the Young's modulus and

Poisson's ratio, was justified uniformly by these correlations for each participant. The density–elasticity relationship was based on mechanical testing data of femur [31, 36]:

$$E = 6850\rho_{app}^{1.49},$$

where E is the elastic modulus in MPa, and ρ_{app} is the apparent density in g/cm^3; all materials were assigned a Poisson's ratio of 0.3. The average elastic modulus was 13.5 GPa (ranged from 2.45 to 17.3 GPa) for the cortical bone.

The finite element and musculoskeletal models were aligned into a common local coordinate system at the hip joint, in which 27 femoral muscle insertion locations from Arnold's model were mapped to surface nodes of the finite element model. The whole model was physiologically constrained (described in the local coordinate system) at: (1) the lateral epicondyle at the anterior–posterior direction; (2) the center of the patellar groove at the anterior–posterior, medial–lateral and vertical directions; and (3) the femoral head contact point at the anterior–posterior, medial–lateral directions [39]. In the analysis, all the joint contact forces and muscle forces were applied as point load for the analysis [39]. The directions and magnitudes of the point load were shown in Fig. 2 and Table 1.

The compressive (minimal principal) and tensile (maximal principal) strains at the whole femur were analyzed during both hip joint contact force peaks (Fig. 3), the distribution of the elastic modulus was plotted in Fig. 4. The whole femoral cross-sections at each 10% of the femur length along the long axis were extracted for each subject. Starting from the proximal end of the femur, the cross-sections were numbered from 1st through 9th. All forces were applied as point loads acting on the surface nodes and resulting strain concentrations were removed from further analysis by discarding nodes and elements in the immediate vicinity of load application [34].

The independent variable was the direction of travel (ascent vs. descent), the main dependent variables were compressive (minimal principal) and tensile (maximal principal) strains of 9 cross-sections of the femur (Fig. 1). The strain was estimated at the two time points during the stance phase that corresponded with the two peak values on the time by hip joint contact force curves. The means of 5 trials for each direction were used for statistical analysis. A repeated-measures ANOVA was used in the analysis, and pairwise t-tests were used to compare the maximum strains on the femoral neck between stair ascent and descent during the 1st and 2nd hip contact force peaks for each cross-section. The related hip joint kinematics and kinetics variables were tested between stair ascent and descent using pairwised t-test. The α level of all tests was set to 0.05 (SPSS, IBM Corp).

For both compressive and tensile strains, the percentage of strain differences between stair ascent and descent was calculated for each cross-section:
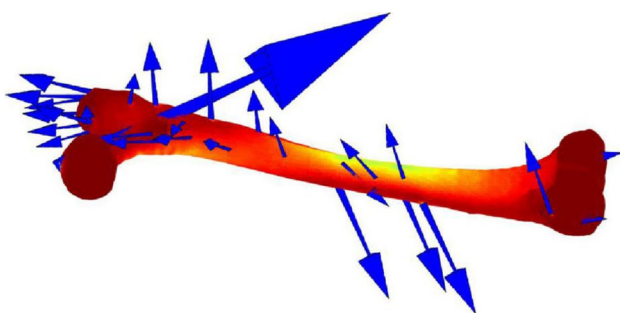

Fig. 2 The applied point loads on the femur model

Table 1 The magnitudes of muscle forces and hip joint contact force acting on the femur model (for one participant), unit in Newtons

Load name	Resultant force	Load name	Resultant force
Hip joint contact force	2264.9	Pectineus	0.1
Gluteus medius (anterior)	228.6	Gluteus maximus (superior)	183.1
Gluteus medius (middle)	196.0	Gluteus maximus (middle)	213.0
Gluteus medius (posterior)	127.0	Gluteus maximus (inferior)	139.9
Gluteus minimus (anterior)	162.3	Iliacus	0.2
Gluteus minimus (middle)	144.0	Psoas	0.1
Gluteus minimus (posterior)	116.5	Quadratus femoris	0.4
Biceps femoris short head	0.4	Gemelli	1.5
Adductor longus	0.1	Piriformis	33.6
Adductor brevis	0.2	Vastus medialis	310.2
Adductor magnus (proximal)	0.1	Vastus intermedius	313.0
Adductor magnus (middle)	0.5	Vastus lateralis	312.2
Adductor magnus (distal)	23.9	Gastrocnemius medial head	9.6
Adductor magnus (ischial)	93.2	Gastrocnemius lateral head	11.7

Fig. 3 The resultant hip contact force during stair ascent and descent, unit BW stands for body weight
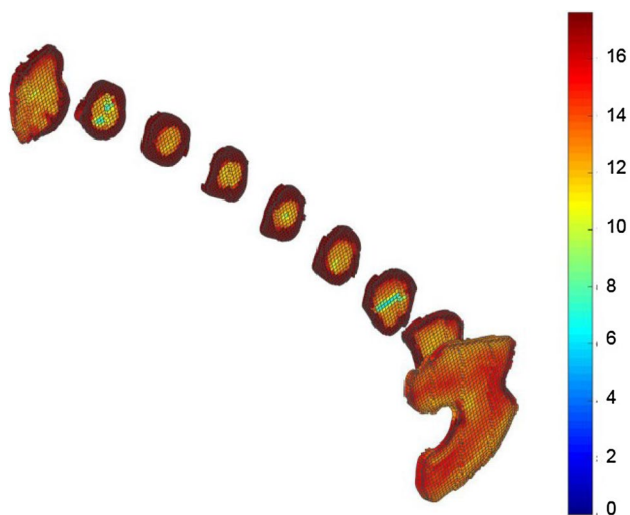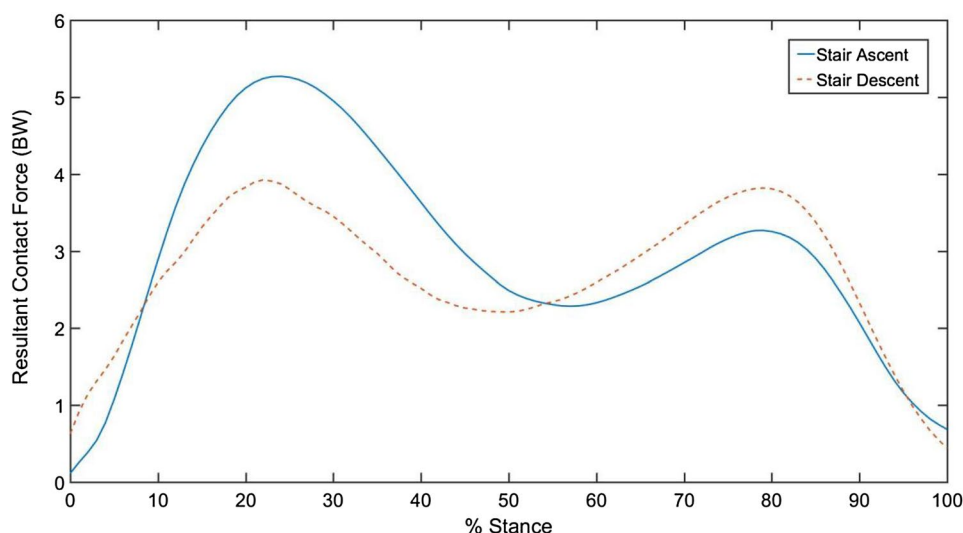

Fig. 4 The distribution of the elastic modulus for 9 cross sections of whole femur (unit: GPa)

$$\%\text{DIFF} = \frac{\text{Strain}_{SD} - \text{Strain}_{SA}}{\text{Strain}_{SD}}.$$

In which %DIFF stands for percentage of strain differences between stair ascent and descent, Strain_{SD} stands for the strains for stair descent, Strain_{SA} stands for the strains for stair ascent.

Results

Hip Joint Kinematics and Kinetics

The hip joint angle patterns for stair ascent and descent were shown during stance phase (Fig. 5). The range of the abduction and adduction (frontal plane) angles were lower than 15° for stair ascent, and lower than 10° for descent. Low range of the internal and external rotation (transverse plane) angles were shown for stair ascent (approximately 10°) and descent (lower than 5°). Large flexion and extension (sagittal plane) angles were shown for stair ascent (approximately 50°) but stair descent remains low range of angles (approximately 5–7°).

The hip joint reaction forces (acting on the femoral head) and moments were shown for stair ascent and descent during stance phase (Figs. 6, 7). For the AP (anterior–posterior) reaction forces, stair ascent produced greater posteriorly directed reaction force than descent for peak 1 (ascent: 0.35 ± 0.059 BW; descent: 0.18 ± 0.091 BW, $P < 0.001$). For the VERT (long axis of the femur) reaction forces, stair descent produced greater downward directed reaction force than descent for peak 1 (ascent: 0.80 ± 0.041 BW; descent: 1.12 ± 0.087 BW, $P < 0.001$), the downward directed reaction force was greater for stair ascent than descent for peak 2 (ascent: 0.96 ± 0.087 BW; descent: 0.73 ± 0.067 BW, $P < 0.001$).

Stair ascent peak extensor moments were statistically greater during ascent than descent (ascent: 0.079 ± 0.021 BWm; descent: 0.026 ± 0.017 BWm, $P < 0.001$). The abduction moments were statistically greater during stair ascent for peak 1 (ascent: 0.10 ± 0.011 BWm; descent: 0.092 ± 0.014 BWm, $P = 0.014$) and 2 (ascent: 0.090 ± 0.011 BWm; descent: 0.070 ± 0.015 BWm, $P < 0.001$).

The hip joint contact forces were reported in a previous study [10], which showed that most components of the hip joint contact force were statistically greater during ascent than descent for the first peak of the contact force, and greater during descent than ascent for the second peak.
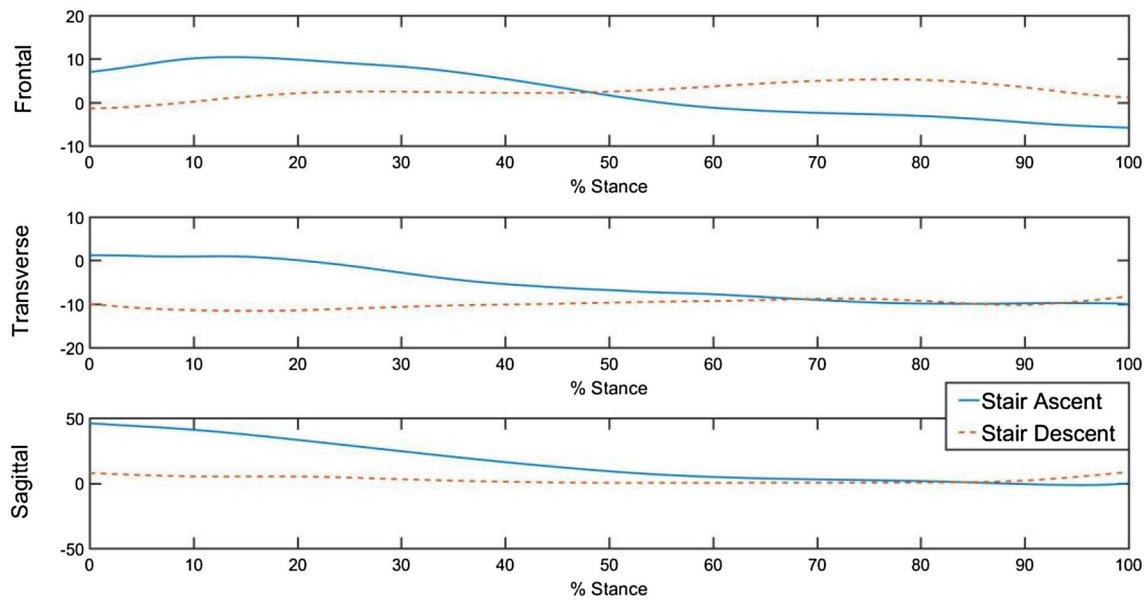
Fig. 5 The patterns of hip joint angles during stair ascent and descent, positive values indicated abduction (frontal plane), internal rotation (transverse plane), and flexion (sagittal plane)
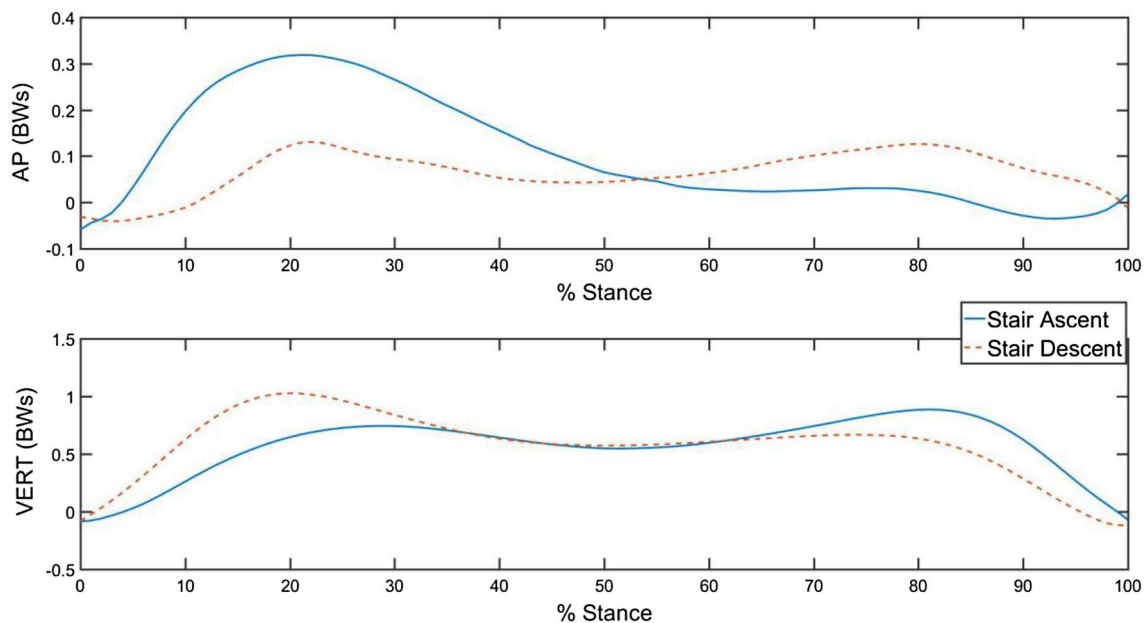

Fig. 6 The patterns of hip joint reaction forces during stair ascent and descent (acting on the femoral head), positive values indicated posterior (AP: anterior–posterior), downward (VERT: long axis of the femur) directions

Femoral Strains

The maximum femoral head deflections in the model were ranged from 1.7 to 3.3 mm for all the participants (the range of axial stiffness was from 1037 to 1230 N/mm), which were within a physiologically realistic range, in particular < 4 mm [39, 41]. The ANOVA tests ($P < 0.021$) showed that there

should be some significant strain differences between stair ascent and descent.

Compressive Strains

The compressive strains are presented for all 9 cross-sections (Table 2). The maximum compressive strain values
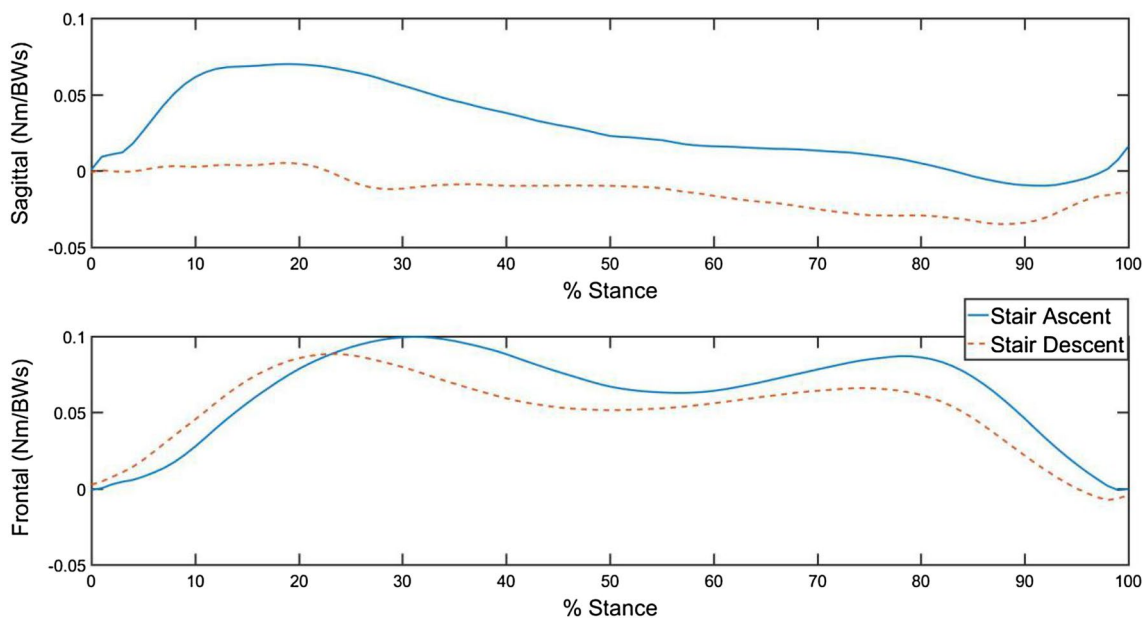
Fig. 7 The patterns of hip joint moments during stair ascent and descent, positive values indicated extension (frontal plane), abduction (sagittal plane)

Table 2 Means (SD) of the compressive strains (in με), and percentage of difference between stair ascent and descent for 9 cross-sections of the femur

Compressive strains

Cross-section	Peak 1			Peak 2		
	Stair ascent	Stair descent	% difference	Stair ascent	Stair descent	% difference
1	− 256.4 (75.0)	− 581.1 (241.8)	**126.64%**[a]	− 274.91 (109.2)	− 510.01 (230.2)	**85.52%**[a]
2	− 460.2 (144.5)	− 1016 (444.1)	**120.77%**[a]	− 483.71 (191)	− 890.41 (411.7)	**84.08%**[a]
3	− 377.4 (131.2)	− 859.6 (398.8)	**127.77%**[a]	− 401.11 (156.4)	− 756.81 (370.2)	**88.68%**[a]
4	− 374.6 (122.0)	− 801.3 (359.2)	**113.91%**[a]	− 388.71 (136.7)	− 706.81 (335.1)	**81.83%**[a]
5	− 324 (103.8)	− 687.6 (309.1)	**112.22%**[a]	− 338.11 (114.7)	− 608.81 (288.4)	**80.06%**[a]
6	− 262.6 (90.2)	− 549.7 (229.2)	**109.33%**[a]	− 273.51 (92.8)	− 491.51 (215.3)	**79.70%**[a]
7	− 163 (67.3)	− 345.5 (159.7)	**111.96%**[a]	− 169.81 (65.4)	− 308.81 (150.6)	**81.86%**[a]
8	− 101.8 (54.5)	− 139.9 (61.4)	**37.43%**[c]	− 93.03 (49.5)	− 137.12 (63.3)	**47.39%**[b]
9	− 99.7 (53.3)	− 208.5 (84.9)	**109.13%**[a]	− 97.51 (42.5)	− 202.41 (83.9)	**107.58%**[a]

Values in bold were significantly different from the corresponding peak between stair ascent and descent

[a]$P < 0.001$

[b]$P < 0.01$

[c]$P < 0.03$

were located at the 2nd cross-section (stair ascent peak 1: − 460.2 ± 144.5 με, peak 2: − 483.7 ± 191.0 με; descent peak 1: − 1016.0 ± 444.1 με, peak 2: − 890.4 ± 441.7 με). The 3rd to 5th cross-sections also maintained high level of compressive strains (ranged from − 324.0 ± 103.8 to − 401.1 ± 156.4 με for stair ascent, from − 608.8 ± 288.4 to − 859.6 ± 398.8 με for descent) and the distal cross-sections had lower compressive strains (ranged

from − 93.0 ± 49.5 to − 273.5 ± 92.8 με for stair ascent, and from − 137.1 ± 63.3 to − 549.7 ± 229.2 με for descent).

Greater compressive strains were found during stair descent at both hip joint contact force peaks (peak 1 and 2). At peak 1, %DIFFs were greater than 120% for the 1st to 3rd cross-sections (proximal regions), and around 110% for the 4th to 7th and 9th cross-sections (shaft and distal regions). These %DIFFs during peak 2 were lower than peak 1 but

showed the similar trend, which were greater than 85% for the 1st to 3rd cross-sections, about 80% for the 4th to 7th cross-sections, and around 110% for the 9th cross-section. All the differences were significant according to the statistical analysis.

The compressive strain concentrations in each cross-section were located at different areas among all the cross-sections (Fig. 8). For both peak 1 and 2, the compressive concentrations were found at the medial area of the 1st–8th cross-sections and the central area of the 9th cross-section, the lateral area strain concentrations were shown for the 2nd–5th cross-sections for stair ascent. For stair descent, the compressive concentrations were at the medial–anterior (M–A) area of the 1st–8th cross-sections and the central area of the 9th cross-section, the lateral–posterior (L–P) area strain concentrations were shown for the 2nd–6th cross-sections.

Tensile Strains

The tensile strains are shown in Table 3. The maximum tensile strain values were located at the 4th cross-section during stair ascent (peak 1: 384.5 ± 115.2 με, peak 2: 399.0 ± 127.0 με), and the 3rd cross-section during descent (peak 1: 754.1 ± 350.0 με, peak 2: 673.2 ± 327.0 με). Cross-sections from 2nd to 5th keep high strain levels during stair ascent and descent (ranged from 336.2 ± 105.4 to 391.8 ± 136.9 με for stair ascent, from 546.9 ± 252.8 to 741.7 ± 333.6 με for descent), and the rest cross-sections (6th to 9th) maintained lower level of tensile strains (ranged from 97.1 ± 53.6 to 271.6 ± 91.1 με for stair ascent, from 128.7 ± 51.8 to 426.5 ± 173.7 με for descent).

Stair descent produced greater tensile strains for most cross-sections at both peak 1 and 2. The %DIFFs for the tensile strains were greater than 80% for the 2nd–5th and
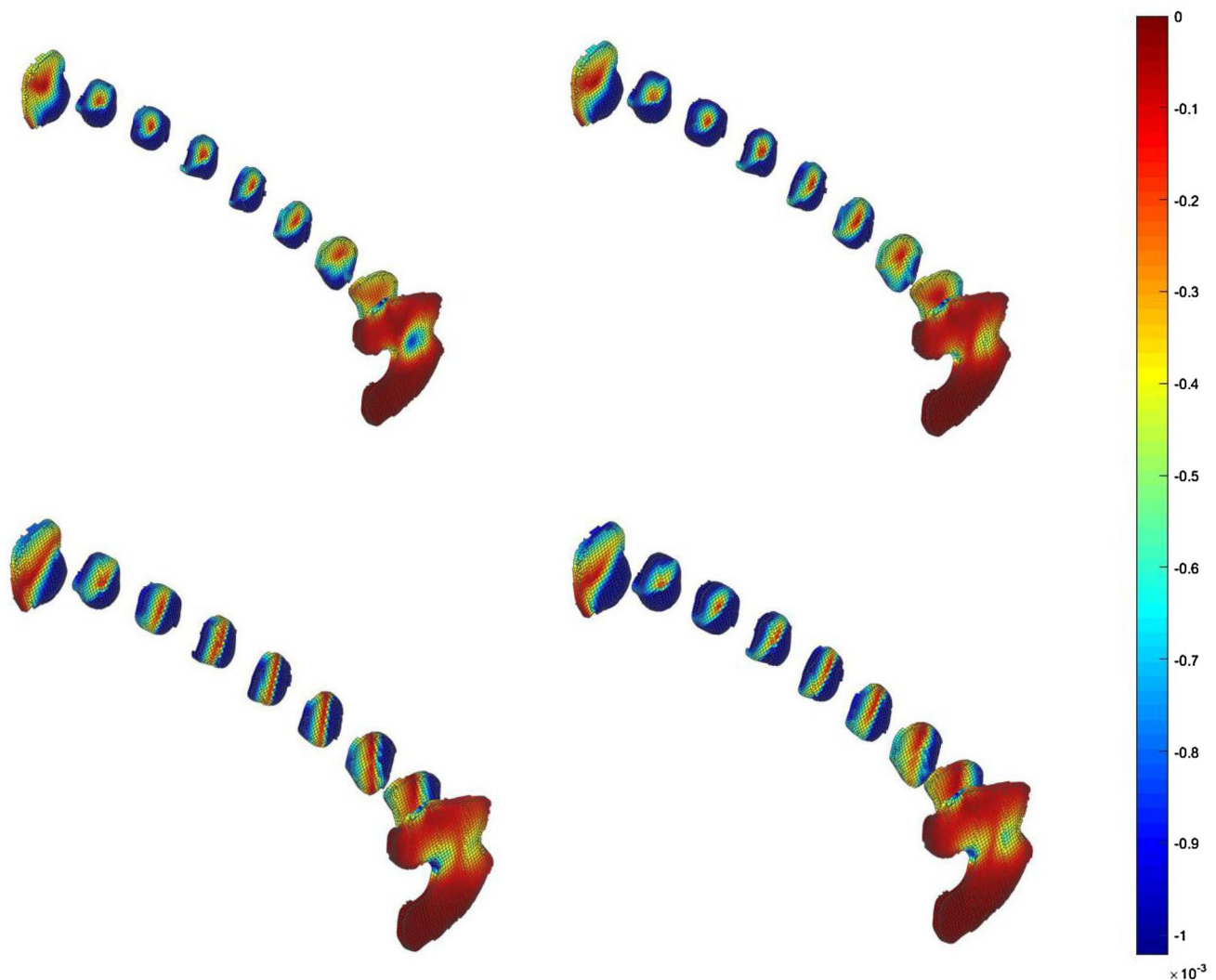

Fig. 8 The compressive strains for 9 cross sections of whole femur, up-left: stair ascent peak 1; up-right: stair ascent peak 2; bottom-left: stair descent peak 1; bottom-right: stair descent peak 2

Table 3 Means (SD) of the tensile strains (in με), and percentage of difference between stair ascent and descent for 9 cross-sections of the femur

	Tensile strains					
	Peak 1			Peak 2		
Cross-section	Stair ascent	Stair descent	% difference	Stair ascent	Stair descent	% difference
1	285.5 (74)	461.3 (188.7)	**61.58%**[a]	280.91 (88.9)	416.41 (178.8)	**48.24%**[a]
2	381.5 (110.1)	741.7 (33.6)	**94.42%**[a]	391.81 (136.9)	662.11 (313.5)	**68.99%**[a]
3	363.4 (114.8)	754.1 (350)	**107.51%**[a]	385.01 (−136)	673.21 (−327)	**74.86%**[a]
4	384.5 (115.2)	724.4 (330.3)	**88.40%**[a]	399.01 (127)	638.81 (309.5)	**60.10%**[a]
5	336.2 (105.4)	612.8 (270)	**82.27%**[a]	342.21 (108.5)	546.91 (252.8)	**59.82%**[a]
6	271.6 (91.1)	426.5 (173.7)	**57.03%**[a]	262.31 (85.4)	390.01 (165.6)	**48.68%**[a]
7	189.2 (79.9)	267.1 (112)	**41.17%**[b]	170.92 (68.5)	248.22 (106.7)	**45.23%**[b]
8	126.2 (70)	128.7 (51.8)	1.98%	101.1 (60)	129.3 (51.2)	27.89%
9	117.6 (69.9)	221.1 (96.5)	**88.01%**[b]	97.12 (53.6)	230.21 (93.5)	**137.04%**[a]

Values in bold were significantly different from the corresponding peak between stair ascent and descent

[a] $P < 0.001$

[b] $P < 0.01$

9th cross-sections; around 60% for the 1st and 6th cross-sections at peak 1. At peak 2 the %DIFFs were lower than peak 1, which were around 60%–75% for the 2nd to 5th and over 135% for the 9th cross-section; for the 1st, 6th and 7th cross-sections were around 50%. Overall, all these presented strain differences were significant according to the statistical analysis.

The tensile strain concentration locations were shown at different areas among all the cross-sections (Fig. 9). For stair ascent, the tensile strain concentration locations were at the lateral area of the 1st–6th cross-sections and the central area of the 9th cross-section, the lateral–posterior (L–P) area strain concentrations were shown for the 7th–8th cross-sections. For stair descent, tensile strain concentrations were at the L–P area for the 1st–8th cross-sections, and the central area of the 9th cross-section.

Discussion

The load analysis of femur could be different compared to the whole thigh segment (inverse dynamic based): the segment load analysis won't count muscular forces since they are internal forces; for femur, the joint forces/moments and the muscular forces attaching to femur are all as external loads in the analysis. Strains represent the total effect of external loads acting on its structure, which represent the material deformation during different load conditions (stair ascent and descent). This study was to investigate the whole femoral strains so the high strain locations on different regions could be detected during stair ascent and descent. Maximum compressive and tensile strains at all 9 femoral cross-sections were compared between stair ascent and descent. For the older population, understanding these strain conditions could be used in reduction of femoral pain and pain related falls, and prevention of femoral fractures.

The compressive strains for 9 cross-sections were much greater for stair descent than ascent since most strain differences were greater than 80%–100%. Among all 9 cross-sections, higher strain values were shown for the proximal to mid-shaft areas. The locations of strain concentrations were similar for all the cross-sections between stair ascent and descent. For most cross-sections the greatest strains were more at medial areas and some other strain concentrations were around lateral areas; the 9th cross-section was approximately around the knee joint surface, the greater compressive strains were at the central area, which may represent the knee joint contact force location. Due to the supporting task for the upper body, the loading type for femur along its long axis could be mainly compressive overall, especially in the medial area, and some tensile in the lateral area [1, 32, 41]. These compressive concentrations could be partially explained by the curvature of the femur [41] and the loading characteristics of the femur: the effect of the torso weight acting on the femoral head and the hip muscle contraction could bend the femur more medially during stair ascent and descent. For the strain concentrations at the lateral or L-P areas, it was shown that the greatest tensile strains were at these similar areas, so part of the compressive concentration might be from the effect of the Poisson ratio (as 0.3).

Tensile strains for the most cross-sections were greater for stair descent than ascent, the strain differences were more than 40%–50%. Along the long axis of the femur, greater tensile strain values were also located at the proximal to mid-shaft of the femur. Tensile strain concentration locations were similar for all cross-sections between stair ascent and descent. Most cross-sections were affected by medially bending effect so the greatest strains were more at lateral
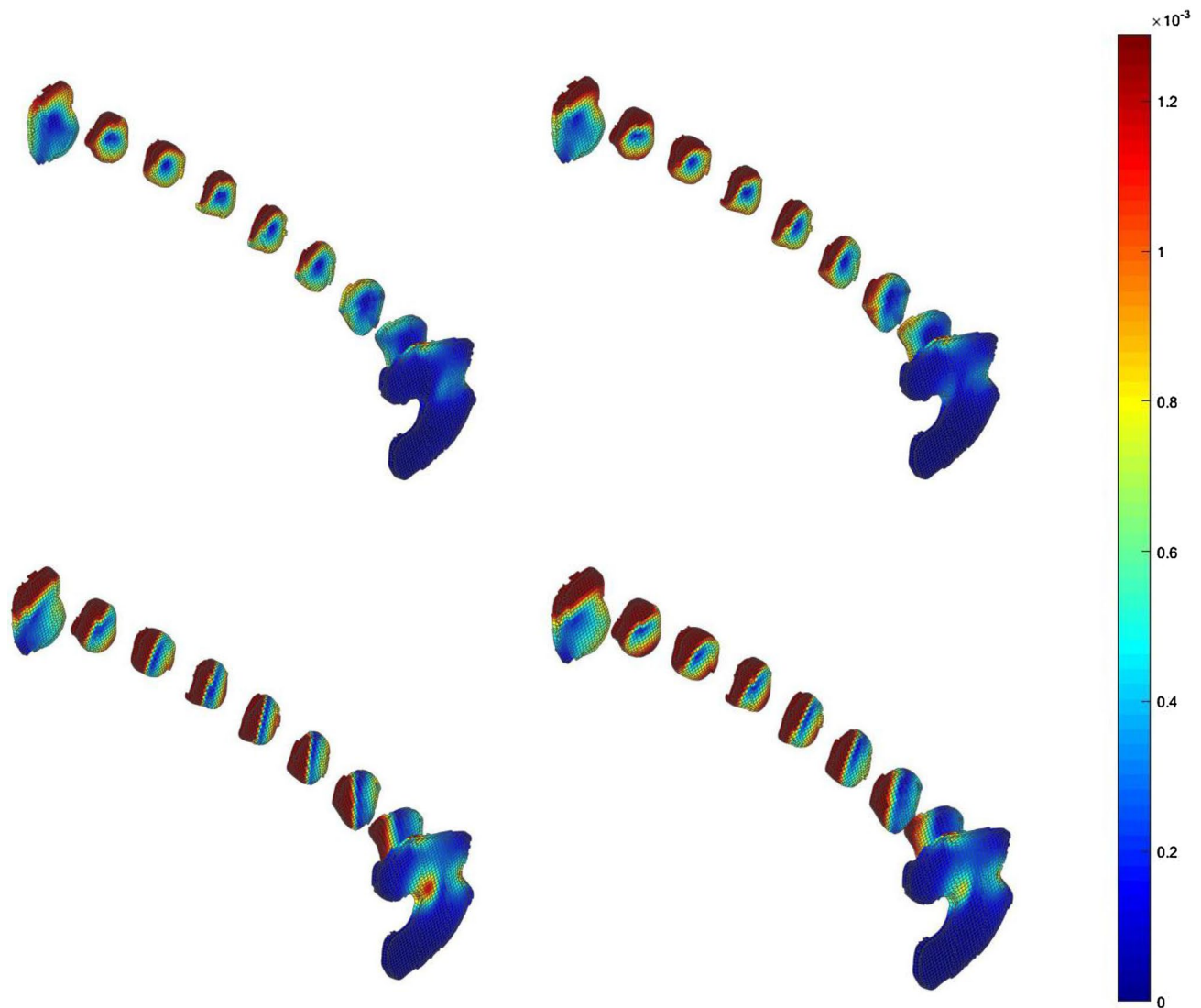
Fig. 9 The tensile strains for 9 cross sections of whole femur, up-left: stair ascent peak 1; up-right: stair ascent peak 2; bottom-left: stair descent peak 1; bottom-right: stair descent peak 2

areas; the knee joint contact force should locate at the central area of the 9th cross-section.

In general, stair descent produced greater strains for the femur than ascent. During stair descent, less muscular activities for the hip/knee extensor and hip abductor muscle were found based on the Arnold's model and static optimization process, the patterns of the estimated muscle forces were similar to the previous studies [10, 18]. This muscle force decrease during stair descent may minimize the muscular protection to the femur [9, 32, 41]. Compared to the previous studies, the principal strains around the sub-trochantic area during stair ascent and descent were much lower than those from Anderson et al. [3] and Aamodt et al. [1] but similar with the walking tests from another study [13], this decrease may partially due to (1) different age groups or population

for the subjects (older group vs. young and older combination, older group vs. patients after surgeries), (2) about 25% lower speed (0.84–0.92 m/s) during stair ascent/descent than walking, (3) the difference in the assigned material property/stiffness.

In this study, both compressive and tensile strains were analyzed for the femur. Using bone strains could help future studies analyze loading conditions in a more comprehensive way for other physical activities, which predicts the risk of stress fractures and tests if alternative methods (gait type change) could reduce stress and strain effectively.

However, this study has some limitations, and future studies could consider to make some adjustments: (1) the femur model does not incorporate any subject-specific imaging to provide information on bone geometry or density, which might

lead to lower loading modulus [25], (2) the body-size scaling across animals [28] may not apply well for the human subjects, using individualized CT or MRI scans could give more accurate prediction, (3) isotropic material properties could lead to overestimation of the tissue stiffness [6], and point load assignment may not accurately reflect the real load conditions, (4) previous studies [13–15, 36] guaranteed the accuracy of the proximal femur model, but the femoral shaft (with medullary canal) was not examined, which may lead to some error in the estimation, (5) in the femoral shaft, trabecular structures and the medullary canal were simplified as the solid elements may have influence on the result, (6) potential errors for the estimation from the musculoskeletal model (underestimation of the muscle co-contraction effect) may still exist, the isometric muscle force testing may help validate the results. For future studies, a more individualized femoral neck model (based on CT scans and anisotropic material properties) and subject-specific musculoskeletal model (based on ultrasound) could be used in the testing. With more accurate information for each individual, the individualized preventative methods or training plan could be developed to enhance the health status of older population.

Availability of Data and Material Not applicable.

Code Availability Not applicable.

Declarations

Conflict of interest Author Timothy Derrick was not involved in the journal's review of, or decisions related to, this manuscript.

Ethics approval ISU IRB # 17-296; approved by Iowa State University Human Subjects Review Board.

Consent to participate All participants signed written informed consent that had been approved by the Iowa State University Human Subjects Review Board.

References

1. Aamodt A, Lund-Larsen J, Eine J, Benum P, Husby OS. In vivo measurements show tensile axial strain in the proximal lateral aspect of the human femur. J Orthop Res. 1997;15(6):927–31.
2. Adler R. Bisphosphonates and atypical femoral fractures. Curr Opin Endocrinol Diabetes Obes. 2016;23(6):430–4.
3. Anderson DE, Madigan ML. Effects of age-related differences in femoral loading and bone mineral density on strains in the proximal femur during controlled walking. J Appl Biomech. 2013;29:505–16.
4. Arnold EM, Ward SR, Lieber RL, Delp SL. A model of the lower limb for analysis of human movement. Ann Biomed Eng. 2010;38(2):269–79.
5. Bergmann G, Deuretzbacher G, Heller M, Graichen F, Rohlmann A, Strauss J, Duda GN. Hip contact forces and gait patterns from routine activities. J Biomech. 2001;34:859–71.
6. Blanchard R, Dejaco A, Bongaers E, Hellmich C. Intravoxel bone micromechanics for microCT-based finite element simulations. J Biomech. 2013;46(15):2710–21.
7. Burstein AH, Reilly DT, Martens M. Aging of bone tissue: mechanical properties. J Bone Jt Surg. 1976;58(1):82–6.
8. Chang MW, Liu HT, Huang CY, Chien P-C, Hsieh H-Y, Hsieh C-H. Location of femoral fractures in patients with different weight classes in fall and motorcycle accidents: a retrospective cross-sectional analysis. Int J Environ Res Public Health. 2018;15(6):1082–90.
9. Cristofolini L. Influence of thigh muscles on the axial strains in a proximal femur during early stance in gait. J Biomech. 1995;28(5):617.
10. Deng C, Gillette JC, Derrick TR. Femoral neck stress in older adults during stair ascent and descent. J Appl Biomech. 2018;34(3):191–8.
11. Duda GN, Heller M, Albinger J, Schulz O, Schneider E, Claes L. Influence of muscle forces on femoral strain distribution. J Biomech. 1998;31(9):841–6.
12. Dunlop DG, Brenkel IJ. The supracondylar intramedullary nail in elderly patients with distal femoral fractures. Injury. 1999;30(7):475–84.
13. Edwards B, Miller R, Derrick T. Femoral strain during walking predicted with muscle forces from static and dynamic optimization. J Biomech. 2016;49(7):1206–13.
14. Edwards B, Schnitzer J, Troy L. Bone mineral loss at the proximal femur in acute spinal cord injury. Osteoporos Int. 2013;24(9):2461–9.
15. Edwards B, Schnitzer J, Troy L. Torsional stiffness and strength of the proximal tibia are better predicted by finite element models than DXA or QCT. J Biomech. 2013;46(10):1655–62.
16. Glitsch U, Baumann W. The three-dimensional determination of internal loads in the lower extremity. J Biomech. 1997;30(11–12):1123–31.
17. Haider IT, Schneider P, Michalski A. Influence of geometry on proximal femoral shaft strains: implications for atypical femoral fracture. Bone. 2018;110:295–303.
18. Hall M, Stevermer CA, Gillette JC. Muscle activity amplitudes and co-contraction during stair ambulation following anterior cruciate ligament reconstruction. J Electromyogr Kinesiol. 2015;25(2):298–304.
19. Hong YNG, Shin CS. Gender differences of sagittal knee and ankle biomechanics during stair to ground descent transition. Clin Biomech. 2015;30(10):1210–7.
20. Jacobs JV. A review of stairway falls and stair negotiation: lessons learned and future needs to reduce injury. Gait Posture. 2016;49:159–67.

21. Kersh ME, Martelli S, Zebaze R, Seeman E, Pandy MG. Mechanical loading of the femoral neck in human locomotion. J Bone Miner Res. 2018;33(11):1999–2006.

22. Keyak JH, Skinner H, Fleming J. Effect of force direction on femoral fracture load for two types of loading conditions. J Orthop Res. 2001;19(4):539–44.

23. Khow KSF, Paterson F, Shibu P. Outcomes between older adults with atypical and typical femoral fractures are comparable. Injury. 2017;48(2):394–8.

24. Lawson E, Madougou S, Chigblo P. Ipsilateral proximal and shaft femoral fractures. Chin J Traumatol. 2017;20(3):155–7.

25. Malandrino A, Fritsch A, Lahayne O, Kropik K, Redl H, Noailly J, Lacroix D, Hellmich C. Anisotropic tissue elasticity in human lumbar vertebra, by means of a coupled ultrasound-micromechanics approach. Mater Lett. 2012;78:154–8.

26. Maravic M, Ostertag A, Cohen-Solal M. Subtrochanteric/femoral shaft versus hip fractures: incidences and identification of risk factors. J Bone Miner Res. 2012;27:130–7.

27. Martelli S, Pivonka P, Ebeling PR. Femoral shaft strains during daily activities: implications for atypical femoral fractures. Clin Biomech. 2014;29(8):869–76.

28. McMahon T. Size and shape in biology. Science. 1973;179:1201–4.

29. Melton LJ, Crowson CS, O'Fallon WM. Fracture incidence in Olmsted County, Minnesota: comparison of urban with rural rates and changes in urban rates over time. Osteoporos Int. 1999;9(1):29–37.

30. Miura T, Kijima H, Ishikawa N, Ebina T, Tani T, Chida S, Suzuki T, Yumto S, Tazawa H, Miyakoshi N, Shimada Y. Comparison of atypical and osteoporotic femoral shaft fractures in the elderly: a multicenter study. Adv Orthop. 2018;2018:1–5.

31. Morgan EF, Bayraktar HH, Keaveny TM. Trabecular bone modulus-density relationships depend on anatomic site. J Biomech. 2003;36(7):897–904.

32. Munih M, Kralj A, Bajd T. Bending moments in lower extremity bones for two standing postures. J Biomed Eng. 1992;14(4):293–302.

33. Nieves JW, Bilezikian JP, Lane JM, Einhorn TA, Wang Y, Steinbuch M, Cosman F. Fragility fractures of the hip and femur: incidence and patient characteristics. Osteoporos Int. 2010;21(3):399–408.

34. Polgar K, Gill HS, Viceconti M, Murray DW, O'Connor JJ. Strain distribution within the human femur due to physiological and simplified loading: finite element analysis using the muscle standardized femur model. Proc Inst Mech Eng C J Eng Med. 2003;217(3):173–89.

35. Rowbotham SK, Blau S, Hislop-Jambrich J, Francis V. Fatal falls involving stairs: an anthropological analysis of skeletal trauma. Forensic Sci Med Pathol. 2018;14(2):152–62.

36. Schileo E, Taddei F, Malandrino A, Cristofolini L, Viceconti M. Subject-specific finite element models can accurately predict strain levels in long bones. J Biomech. 2007;40(13):2982–9.

37. Sivananthan S, Sherry E. Mercer's textbook of orthopaedics and trauma. 10th ed. New York City: Oxford Univ Press; 2012.

38. Smektala R, Endres HG, Dasch B, Maier C, Trampisch HJ, Bonnaire F, Pientka L. The effect of time-to-surgery on outcome in elderly patients with proximal femoral fractures. BMC Musculoskelet Disord. 2008;9(1):171.

39. Speirs AD, Heller MO, Duda GN, Taylor WR. Physiologically based boundary conditions in finite element modelling. J Biomech. 2007;40(10):2318–23.

40. Streubel PN, Ricci WM, Wong A, Gardner MJ. Mortality after distal femur fractures in elderly patients. Clin Orthop Relat Res. 2011;469(10):1188.

41. Taylor ME, Tanner KE, Freeman MA, Yettram AL. Stress and strain distribution within the intact femur: compression or bending? Med Eng Phys. 1996;18(2):122–31.

42. Van Sint JS. The VAKHUM project: virtual animation of the kinematics of the human. Theor Issues Ergon Sci. 2005;6(3–4):277–9.

43. Vaughan C, Davis B, O'Connor J. Dynamics of human gait. Champaign: Human Kinetics; 1992.

44. Viceconti M, Taddei F, Cristofolini L, Martelli S, Falcinelli C, Schileo E. Are spontaneous fractures possible? An example of clinical application for personalised, multiscale neuro-musculoskeletal modelling. J Biomech. 2012;45(3):421–6.

45. Yu B, Gabriel D, Noble L, An KN. Estimate of the optimum cutoff frequency for the Butterworth low-pass digital filter. J Appl Biomech. 1999;15(3):318–29.